CONTROL STRATEGY FOR MULTI-MODULE PARALLEL CONVERTER SYSTEM [1]

B. Choi, B.H. Cho, R.B. Ridley and F.C. Lee

Virginia Power Electronics Center
The Bradley Department of Electrical Engineering
Virginia Polytechnic Institute and State University
Blacksburg, Virginia 24061

ABSTRACT

The control strategy for a multi-module converter system for high-current low-voltage applications is investigated. The system consists of several converter modules in parallel to effectively deliver a high-current output. A multi-stage output filter is employed to efficiently attenuate the ripple and high-frequency noise. In addition to output voltage and inductor current feedbacks, a feedback from the intermediate filter stage is employed to optimize the transient response in the event of failure of a converter module, and also to improve the other closed-loop performances of the system. Based on the small-signal analysis, a systematic control-loop design procedure for optimal performance of the system is presented.

1. INTRODUCTION

With rapid advance of VLSI technologies, there are increasing demands for power supplies which must provide high-current low-voltage output efficiently and reliably. Many applications require hundreds of amperes of load current at output voltage of 5 V or less, with stringent ripple and noise specifications. The high-current requirement is best met by using parallel converter modules with current mode control [1]. The load current is equally distributed among converter modules, thereby improving reliability with reduced current stress of the switching devices. Moreover, the modular approach provides fault-tolerance for the system in the event of failure of a converter module. Finally, with an appropriate phase shift among the switching sequence of converter modules, the switching ripples of the individual converter modules cancel each other, greatly reducing the input and output ripple.

In high-current applications, it is desirable to add a common secondary LC filter between intermediate bus (output of converter module) and the output of the system, to meet the stringent ripple and noise specifications. Reference [2] has shown that an efficient secondary LC filter can be designed to provide good attenuation of the switching ripple, while maintaining adequate stability margins under a wide range of capacitive loadings.

This paper presents a systematic control-loop design procedure for a multi-module converter system with a secondary LC filter. To facilitate the control-loop design, an equivalent single-module model for a multi-module converter system is developed. Having the same closed-loop performance as the original system, the single-module model greatly simplifies the analysis and design of the system.

A three-loop control scheme is proposed. In addition to the output and inductor-current feedbacks, the control scheme employs a feedback from the first-stage filter capacitor (the summing point where all converter modules are merged) in order to improve the transient response due to the failure of a converter module (hereafter referred to as "module-failure response") and the other closed-loop performances. Design procedures of a three-loop control are formulated, which significantly improve the transient responses and the small-signal performances of the system. The advantages of the proposed three-loop control over conventional two-loop control are demonstrated by small-signal analysis and large-signal simulations.

2. EQUIVALENT SINGLE-MODULE MODEL

2.1 Multi-module converter system

Figure 1 shows a schematic diagram of a three-module converter system with the proposed control scheme. The system consists of three buck converter modules in parallel, a common LC filter (L_2 and C_2), and an output voltage feedback circuit, F_R . Each converter module contains a power stage, a pulse width modulation (PWM) block, and two inner feedback circuits: the current sensing network, CIC, for the inductor current (on-time switch current) feedback, and F_L for the capacitor voltage feedback from power stage. The inner feedback from the power stage capacitor is defined as local voltage feedback, and the outer feedback from the output is defined as remote voltage feedback.

[1] The work was supported by the International Business Machines Co., Kingston NY, and by the Virginia Center for Innovative Technology, Technology Development Center for Power Electronics.

CH2873-8/90/0000-0225 $1.00

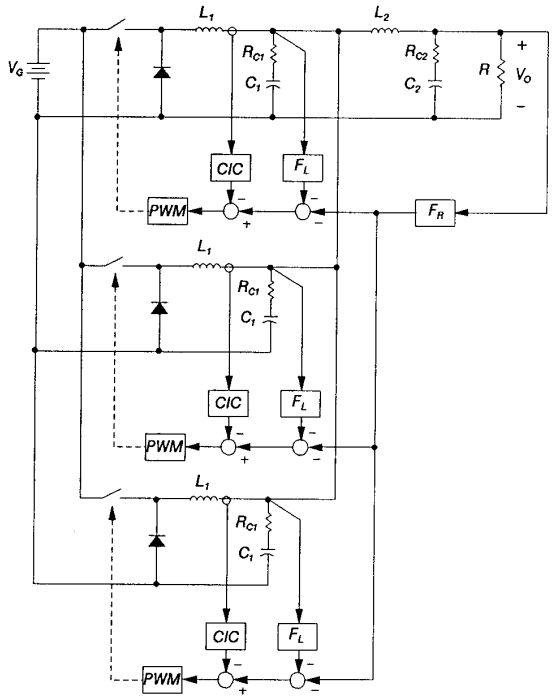

Fig. 1. Three-module converter system with a three-loop control: $L_1 = 12\mu H$ $L_2 = 0.5\mu H$ $C_1 = 867\mu F$ $C_2 = 12000\mu F$ $R_{C1} = 21m\Omega$ $R_{C2} = 6m\Omega$ $R = 0.05\Omega$ $V_G = 12V$ $V_O = 5V$ $f_s = 100kHz$

2.2 Small-signal model of the system

Figure 2 shows the small-signal model of the system obtained using two recently proposed analysis techniques: the PWM switch model [3,4] and the continuous-time small-signal model for a current mode control [5]. An active-passive switch pair of the power stage is replaced with its small-signal PWM switch model. The PWM block and the current sensing network are replaced with their small-signal models, recently proposed in [5]. The modulator gain of PWM block is given by [5]:

$$F_M = \frac{\hat{d}}{\hat{v}_c} = \frac{1}{(S_n + S_e)T_s} \tag{1}$$

where S_n, S_e and T_s are the on-time slope of the current-sense waveform, the slope of an external ramp, and the switching period, respectively. The current sensing network is replaced with a single gain block F_I given by:

$$F_I = R_i H_e(s) \tag{2}$$

R_i is the current sensing network gain, and $H_e(s)$ represents the sampling action of the current mode control, which can be approximated by [5]:

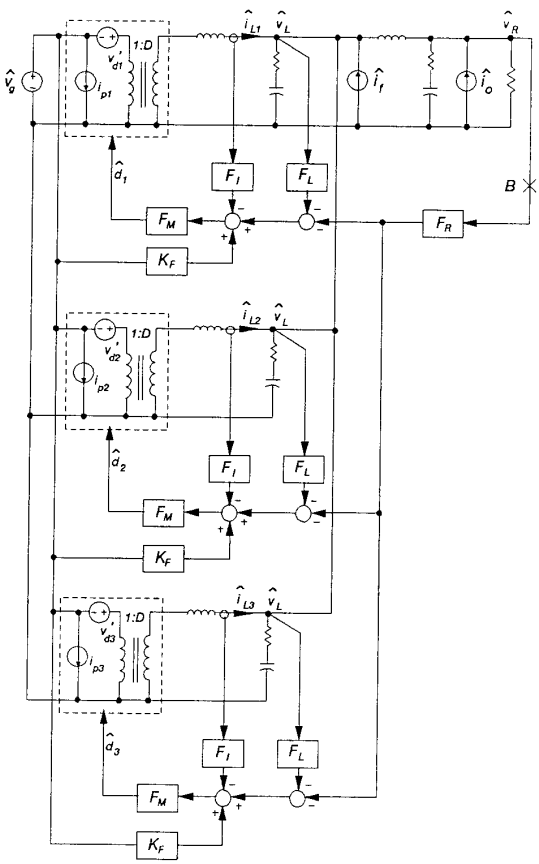

Fig. 2. Small-signal model of system: $v_{dk}' = \frac{V_G}{D} d_k$ $i_{pk} = I_{Lk} d_k$ (k = 1,2,3) where I_{Lk} represents DC inductor current of converter module.

$$H_e(s) \simeq 1 + \frac{s}{\omega_n Q_z} + \frac{s^2}{\omega_n^2} \tag{3}$$

where

$$Q_z = \frac{-2}{\pi} \qquad \omega_n = \frac{\pi}{T_s} \tag{4}$$

K_F represents the feedforward gain from the input voltage. This gain path is created by feedback of the inductor current, the slope of which depends upon the input voltages of the power stage. For a buck converter, this gain is given by [5]:

$$K_F = \frac{\hat{v}_c}{\hat{v}_g} = -\frac{DT_s R_i}{L_1}\left[1 - \frac{D}{2}\right] \tag{5}$$

There is another gain path from the output voltage of the power stage, which represents the dependency of the inductor current slope on the output voltage [5]. However, in most practical applications, this feedback gain is negligible compared to the local voltage feedback compensation,

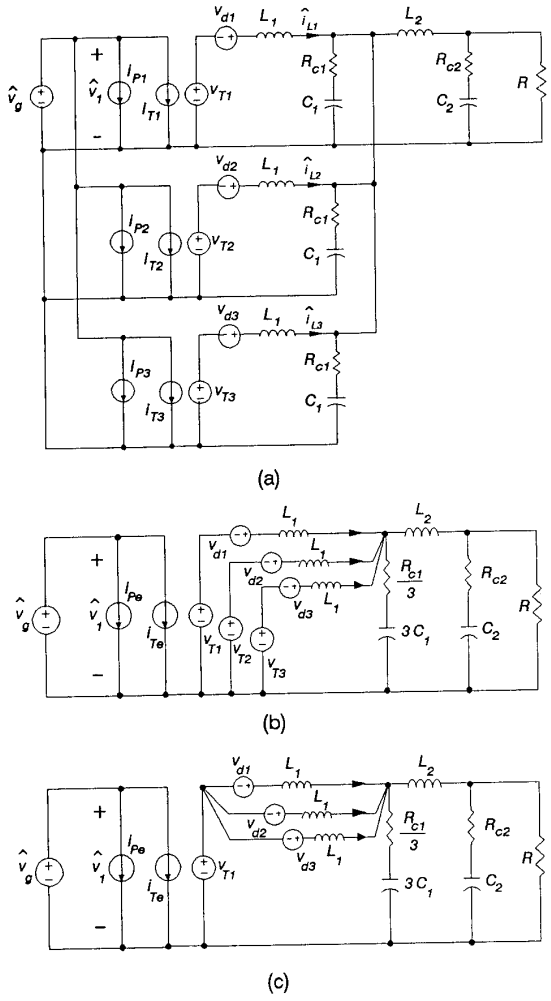

Fig. 3. Simplification of power stage: (a) Modified power stage model $i_{Tk} = Di_{Lk}$ $v_{Tk} = Dv_1$ $v_{dk} = V_G d_k$ (k = 1,2,3) (b) Elimination of common current sources $i_{Pe} = i_{P1} + i_{P2} + i_{P3}$ $i_{Te} = i_{T1} + i_{T2} + i_{T3}$ (c) Elimination of common voltage sources

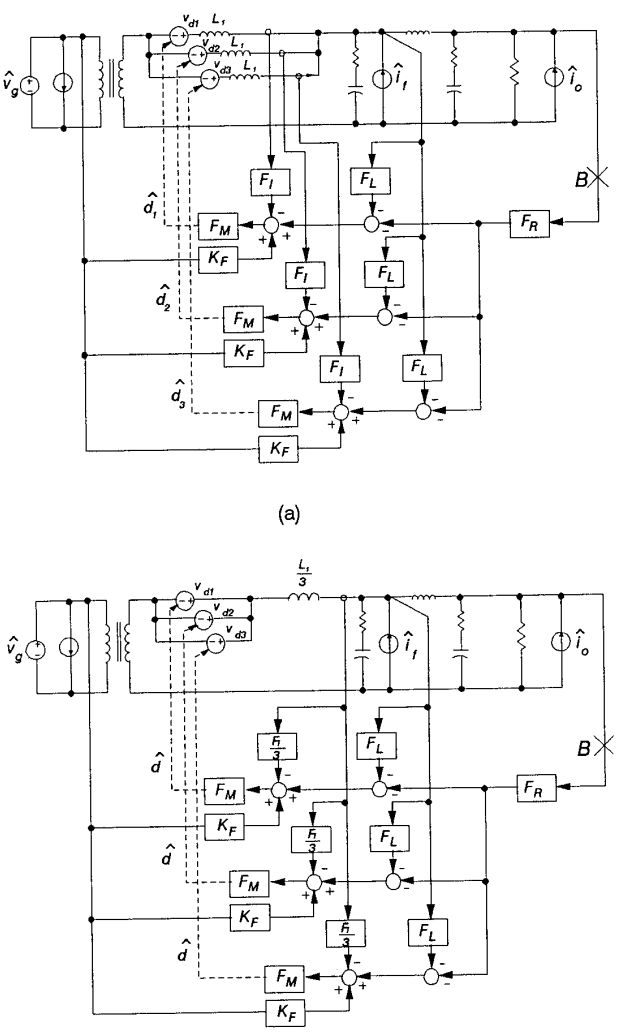

Fig. 4. Derivation of an equivalent single-module model: (a) Small-signal model using the simplified power stage model (b) Further simplification using $d_1 = d_2 = d_3 \equiv d$

F_L . Thus, this gain is not included in the small-signal model. Small-signal sources, v_g and i_o represent the small-signal disturbance of the input voltage and load current, respectively. The additional current source, i_f , represents the current disturbance coming from the individual converter modules. For each converter module, the control variable, d_k, is derived from the three feedback signals v_R , v_L , i_{Lk} $(k = 1,2,3)$, which will be referred to as remote voltage, local voltage, and inductor current, respectively. To characterize the module-failure response systematically, a transfer function called trans-impedance is defined as $Z_T \equiv v_R/i_f$, representing the output voltage response due to the current disturbance coming from the converter modules. The other closed-loop performances include:

- audio-susceptibility $A_U \equiv \hat{v}_R/\hat{v}_g$;
- output impedance $Z_O \equiv \hat{v}_R/\hat{i}_o$; and
- loop gain measured at B.

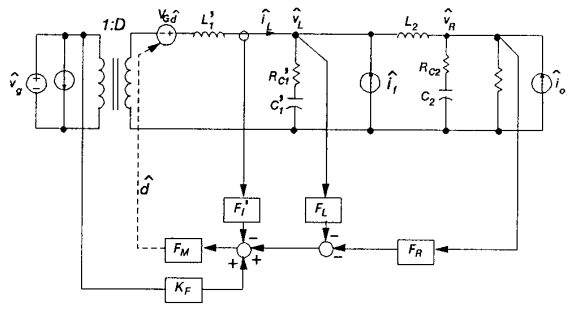

Fig. 5. Equivalent single-module model $L_1' \equiv \frac{L_1}{3}$ $R_{C1}' \equiv \frac{R_{C1}}{3}$ $C_1' \equiv 3C_1$ $F_I' \equiv \frac{F_I}{3}$

2.3 Equivalent single-module model

The small-signal system model of Fig. 2 is successively simplified to yield a single-module converter model, which has the same closed-loop performance as the original system. This equivalent single-module model can be used for analysis and control-loop design purpose.

Figure 3 illustrates the simplification of the power stage. In Fig. 3(a) the power stage model is slightly modified; the ideal transformer is replaced with a pair of current source i_{Tk} and voltage source v_{Tk}, and the dependent voltage source v_{dk}' is moved to the secondary side of the transformer and relabled as v_{dk} (k = 1,2,3). The current sources i_{P1}, i_{P2}, i_{P3} and i_{T1}, i_{T2}, i_{T3} in Fig. 3(a) are appropriately combined to yield Fig. 3(b). Three identical voltage sources in Fig. 3(b), v_{T1} v_{T2} v_{T3}, are combined, and subsequently v_{T2} and v_{T3} are removed to yield Fig. 3(c).

Figure 4(a) shows the system model with the simplified power stage, where a pair of current and voltage sources, i_{Te} and v_{T1}, are substituted again by an ideal transformer. Since the closed-loop performances of a multi-module converter system are determined by the small-signal sources v_g, i_f, i_o and the injection signal at B, the only considerations in deriving an equivalent single-module model are the system response due to these small-signal sources. Due to the symmetry of the system, d_1, d_2 and d_3 are identical when v_g, i_f, i_o and the injection signal at B are concerned. As a result, three dependent voltage sources, v_{d1}, v_{d2}, and v_{d3}, are the same, and the inductors of converter modules can be combined to yield Fig. 4(b). In Fig. 4(a), the output of the current sensing network of each converter module is given by:

$$\frac{F_I}{L_1}\int v_{L1}dt \qquad (6)$$

Since the inductor is divided by three in Fig. 4(b), the current sensing network gain should also be divided by three, to produce the same output voltage as (6). With this appropriate scaling of the current sensing network gain, the PWM gain F_M and the feedforward gain K_F remain the same in Figs. 4(a) and 4(b).

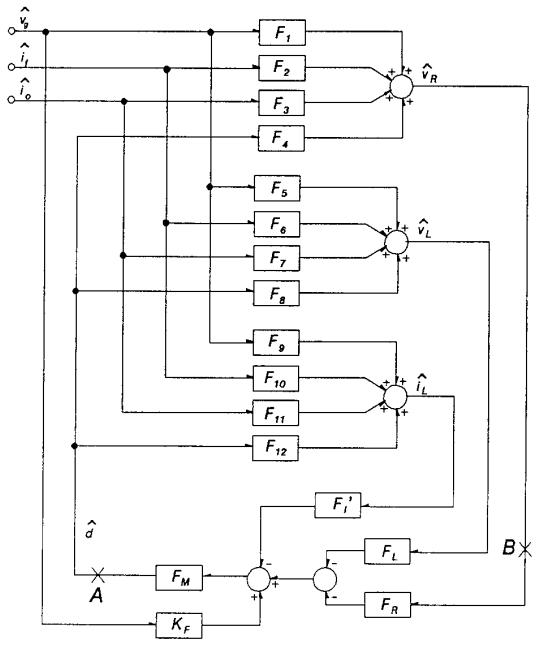

Fig. 6. Small-signal block diagram of system

As the last step, the redundant voltage sources v_{d2} and v_{d3}, together with their associate feedback controllers, are removed, resulting in the equivalent single-module model of Fig. 5. The DC current of the single-module model is the sum of the DC currents of the three converter modules, but the small-signal characteristics of a buck converter are independent of this current. It is important to note that the single-module model is equivalent to the original model only when the loop gain measured at B, audio-susceptibility, output impedance, and trans-impedance are concerned. Apart from that they are entirely different systems; one is a multi-module converter, and the other is a single-module converter.

The design procedures of the multi-module converter system using its equivalent single-module model are:

1. Derive the equivalent single-module model through the appropriate scaling of the common power stage parameters.
2. Design the current sensing network gain and the modulator gain of PWM block (external ramp slope) for the single-module model.
3. Optimize the feedback compensations, F_L and F_R, for the single-module model (this step will be discussed in Section 3).
4. Multiply the current sensing network gain (obtained in 2) with the number of modules to obtain the equivalent gain for the multi-module converter system.

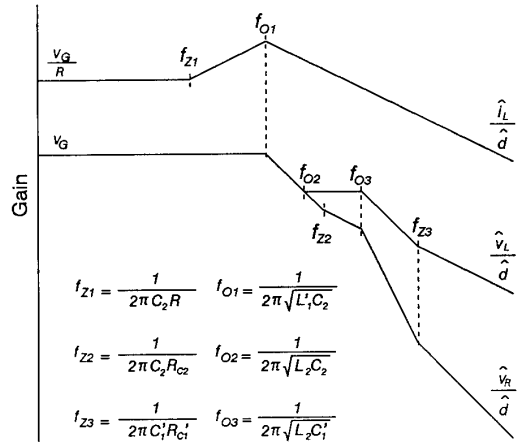

Fig. 7. Asymptotic plots of open-loop transfer functions

3. THREE-LOOP CONTROL

3.1 Open-loop analysis

Figure 6 shows a block diagram representation of the equivalent single-module model of Fig. 5. Transfer functions from the control variable, d, to various feedback signals can be derived from Fig. 5:

$$F_4 = \frac{\hat{v}_R}{\hat{d}} \simeq \frac{V_G[1 + sC_1'R_{C1}']}{[1 + s(C_2R_{C2} + L_1'/R) + s^2L_1'C_2]} \cdot \frac{[1 + sC_2R_{C2}]}{[1 + sC_1'(R_{C1}' + R_{C2}) + s^2L_2C_1']} \quad (7)$$

$$F_8 = \frac{\hat{v}_L}{\hat{d}} \simeq \frac{V_G[1 + sC_1'R_{C1}']}{[1 + s(C_2R_{C2} + L_1'/R) + s^2L_1'C_2]} \cdot \frac{[1 + s(L_2/R + C_2R_{C2}) + s^2L_2C_2]}{[1 + sC_1'(R_{C1}' + R_{C2}) + s^2L_2C_1']} \quad (8)$$

$$F_{12} = \frac{\hat{i}_L}{\hat{d}} \simeq \frac{V_G[1 + sC_2R]}{R[1 + s(C_2R_{C2} + L_1'/R) + s^2L_1'C_2]} \quad (9)$$

with assumptions $L_1' >> L_2$, $C_2 >> C_1'$ and $R >> R_{C1}', R_{C2}$. These assumptions not only make the analysis tractable, but also are a good design practice in order to minimize the detrimental effects of the secondary filter, such as the high-frequency peaking of the output impedance and the possible instability problem with capacitive loadings. With $C_2 >> C_1'$, the system maintains adequate stability margins with capacitive loadings, and eliminates high-frequency peaking of the output impedance [2]. With $L_1' >> L_2$, the control-to-inductor current transfer function can be simplified to a second order given by (9).

Figure 7 shows the asymptotic plots of the transfer functions given by (7), (8) and (9). The control-to-inductor current transfer function is the same as that of the converter with a single-stage output filter of L_1' and C_2, having a first-order slope (-1 slope) with the maximum phase delay of 90°. This desirable property can be used to improve the system performance in a way similar to a conventional current-mode control. The control-to-remote voltage transfer function has two resonances, the first determined by L_1' and C_2 (f_{o1}), and the second determined by L_2 and C_1' (f_{o3}). In control-to-local voltage transfer function, there are the additional complex zeros determined by L_2 and C_2 (f_{o2}) besides two resonances found previously. Due to these complex zeros, the transfer function has the larger mid-frequency gain and can be effectively used to enhance the system performances, as will be illustrated in Section 5.

3.2 Three-loop control

Figure 8 illustrates the principle of the three-loop control in comparison with that of a conventional two-loop control [2]. For the two-loop control, the feedback signals are derived from the first inductor current and the output voltage. This control scheme is illustrated in Fig. 8(a) in terms of two individual feedback loops: current loop and voltage loop [6]. The current loop denotes the feedback loop created by the inductor current feedback, and the voltage loop denotes the feedback path created by the output voltage feedback. With incorporation of $H_e(s)$, which represents the sampling action of the current mode control, the high-frequency characteristics of current loop differ significantly from those found in [7,8]. The complex right half plane zeros give the extra phase delay at half the switching frequency, and an increase in gain [5]. Considering this, generally, the crossover frequency of the current loop should be smaller than that recommended by [7,8].

The three-loop control is illustrated in Fig. 8(b), where current loop T_i, local loop T_L, and remote loop T_R represent the individual feedback loops associated with three feedback signals:

$$T_i \equiv F_M F_{12} F_I' \quad (10)$$

$$T_L \equiv F_M F_8 F_L \quad (11)$$

$$T_R \equiv F_M F_4 F_R \quad (12)$$

At low frequencies, the remote loop is dominant, as seen previously. In the mid-frequency band, however, the local loop is dominant in order to minimize any detrimental effect of the resonance due to L_2 and C_1', as will be illustrated in Section 5. At high frequencies, the current loop is dominant, thus realizing the full benefits of current mode control.

The feedback compensations of the three-loop control are summarized as follows:

- Current sensing network gain : R_i

  For the full benefits of the current mode control, R_i should be selected to provide a sufficiently high crossover frequency for T_I.

- Local loop compensation : $\frac{K_L}{(1 + \frac{s}{\omega_p})}$

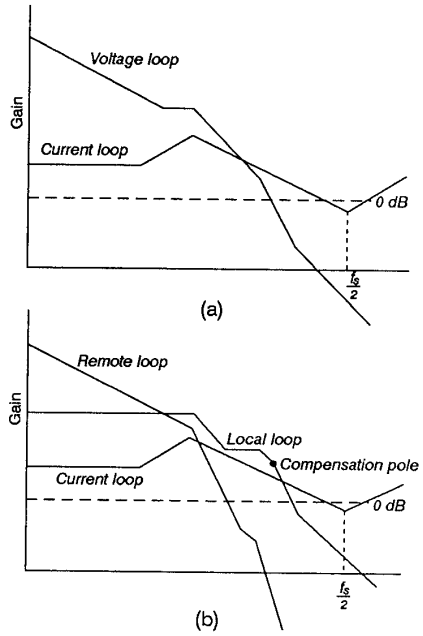

Fig. 8. Principle of a three-loop control: (a) Two-loop control (b) Three-loop control

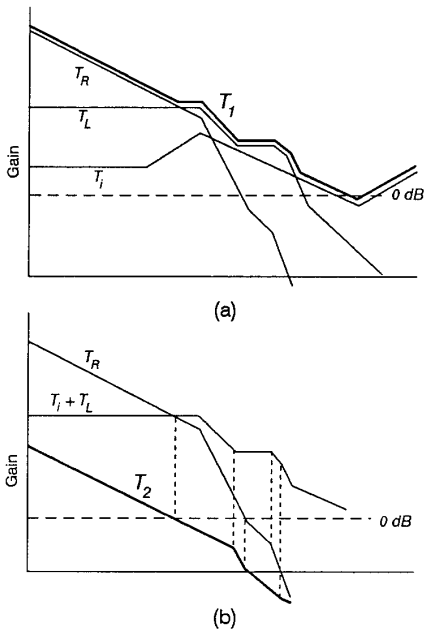

Fig. 9. Loop gains: (a) Overall loop gain (b) Outer loop gain

K_L should be selected to provide the sufficient mid-frequency gain of T_L, while maintaining the dominance of current loop at high frequencies. A pole, ω_p, is placed after the resonance between L_2 and C_1' to reduce the high-frequency gain.

- Remote loop compensation : $\frac{K_R}{s}$

  An integrator is employed to provide a good DC regulation of the output voltage. The integrator gain, K_R, determines the low-frequency attenuation of the closed-loop transfer functions.

4. SMALL-SIGNAL ANALYSIS

4.1 Loop gain analysis

Since the system loop gains are directly or indirectly related to small-signal performances of a converter [6,7], they can be conveniently used to evaluate the closed-loop performances and to assist designing the system. Among many possible loop gains in Fig. 6, two loop gains are most useful: the overall loop gain T_1, measured at A, and the outer loop gain T_2, measured at B [6]:

$$T_1 = T_i + T_L + T_R \tag{13}$$

$$T_2 = \frac{T_R}{1 + T_i + T_L} \tag{14}$$

Figure 9(a) shows the overall loop gain, T_1, with its associated individual feedback loops, T_i, T_L, T_R. As a vector sum of the individual feedback loops, T_1 follows the largest component of the individual feedback loops at any given frequency, and provides the effective means of optimizing the feedback compensations. The compensation for T_i can be designed to maximize the crossover frequency of T_1. The compensation for T_L can be designed to boost the mid-band gain of T_1, while maintaining the dominance of T_i at high frequencies.

Figure 9(b) shows the outer loop gain, T_2. As a ratio of T_R and $1 + T_i + T_L$, the loop gain has relatively small magnitude and crossover frequency. Even though the overall loop gain can be conveniently used during the design process with the equivalent single-module model, in actual system there is no single point where T_1 can be measured. The outer loop gain, on the other hand, can be easily measured to confirm design results and to evaluate the stability of the system.

The relative stability of the system can be evaluated from the phase and gain margins of these loop gains. The implications of the phase and gain margins of these loop gains are as different as are their definitions. The stability margins of T_1 indicate the relative stability of the system with respect to a simultaneous variation of $T_i + T_L + T_R$. The stability margins of T_2 can be interpreted as additional gain increase or phase delay, which can be introduced in T_R when T_i and T_L remain the same.

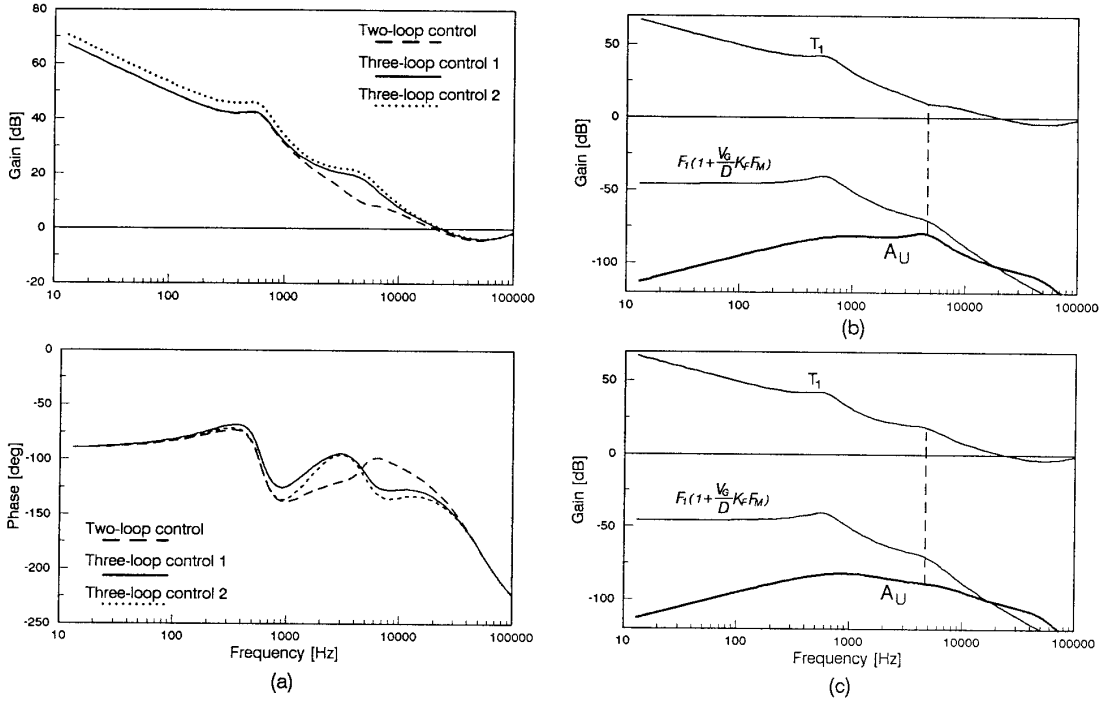

Fig. 10. Performances of a three-loop controlled converter: (a) Overall loop gain (b) Audio-susceptibility and overall loop gain (two-loop control) (c) Audio-susceptibility and overall loop gain (three-loop control 1)

4.2 Closed-loop performance and local voltage feedback

From the small-signal block diagram of Fig. 6, the audio-susceptibility can be derived as:

$$A_U = \frac{F_1 + K_F F_M F_4 + T_i(F_1 - \frac{F_9 F_4}{F_{12}}) + T_L(F_1 - \frac{F_5 F_4}{F_8})}{1 + T_i + T_L + T_R} \quad (15)$$

From the power stage model of Fig. 5, it can be shown:

$$\frac{F_1}{F_4} = \frac{F_5}{F_8} = \frac{F_9}{F_{12}} = \frac{D}{V_G} \quad (16)$$

which simplifies (15) to:

$$A_U = \frac{F_1(1 + \frac{V_G}{D} K_F F_M)}{1 + T_i + T_L + T_R} \quad (17)$$

This relatively simple expression of the audio-susceptibility is an inherent property of a buck converter. In boost or buck/boost converters, the third and fourth terms of the numerator do not vanish simultaneously.

From Fig. 6, trans-impedance can be derived as:

$$Z_T = \frac{F_2 + T_i(F_2 - \frac{F_{10} F_4}{F_{12}}) + T_L(F_2 - \frac{F_6 F_4}{F_8})}{1 + T_i + T_L + T_R} \quad (18)$$

From Fig. 5, it can be shown that:

$$\frac{F_6}{F_8} = \frac{F_2}{F_4} = \frac{sL_1'}{V_G} \quad (19)$$

which simplifies (18) to:

$$Z_T = \frac{F_2 + T_i(F_2 - \frac{F_{10} F_4}{F_{12}})}{1 + T_i + T_L + T_R} \quad (20)$$

Finally, the output impedance is given by:

$$Z_O = \frac{F_3 + T_i(F_3 - \frac{F_{11} F_4}{F_{12}}) + T_L(F_3 - \frac{F_7 F_4}{F_8})}{1 + T_i + T_L + T_R} \quad (21)$$

The effects of the local voltage feedback can be investigated from (17), (20), and (21). The local voltage feedback directly attenuates the audio-susceptibility and trans-impedance since T_L appears only in the denominator of (17) and (20). As will be illustrated in the next section, these transfer functions are significantly improved with the local voltage feedback. In the output impedance, however, T_L appears in both numerator and denominator, indicating that its effect is not as significant as in previous cases.

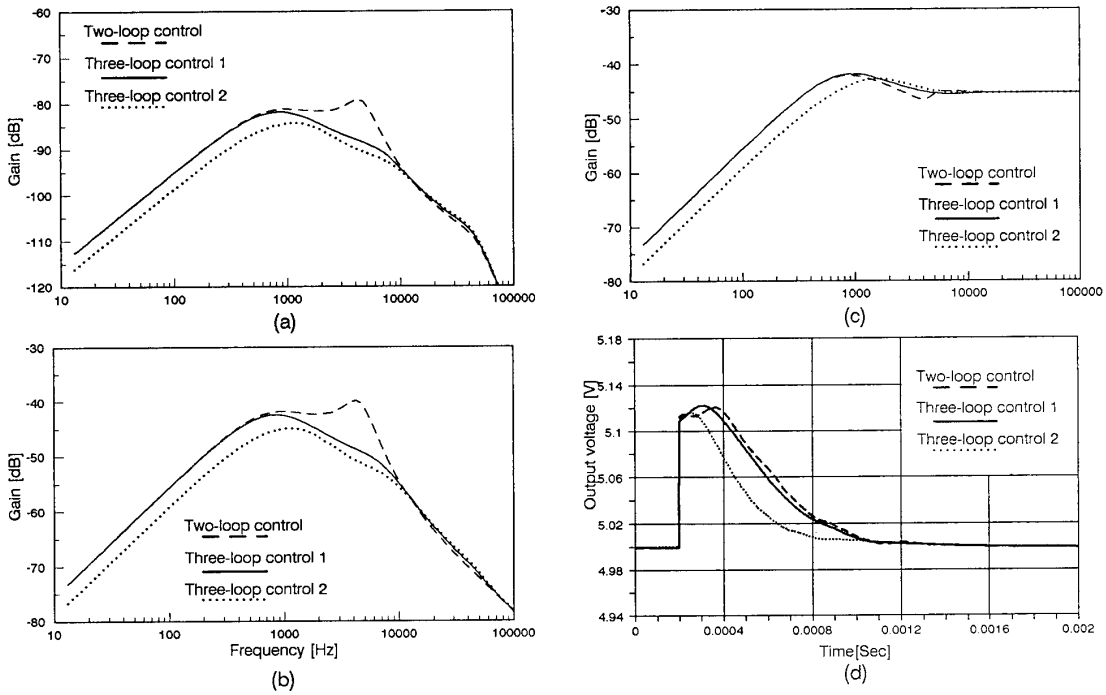

Fig. 11. Performances of a three-loop controlled converter: (a) Audio-susceptibility (b) Trans-impedance (c) Output impedance (d) Step load response (step = 20A)

5. PERFORMANCE OF THE THREE-LOOP-CONTROLLED CONVERTER

5.1 Comparison with two-loop control

First, to demonstrate the benefits of the local voltage feedback, the closed-loop performance of the three-loop-controlled converter is compared with that of a two-loop-controlled converter. For the two-loop control, the control-loop is optimally designed following the procedures explained in [2]. On the other hand, for three-loop control, the control-loop is intentionally designed to have the same low- and high-frequency characteristics as those of the two-loop control. This design is referred to as **three-loop control 1** in Figs. 10 through 13.

Overall loop gains are compared in Fig. 10(a). For the three-loop control, the mid-frequency gain is boosted by absorbing the resonance between L_2 and C_1' with the local voltage feedback, while maintaining the similar stability margins to those of a two-loop control. The phase delay and gain increase at half the switching frequency are a result of the sampling action of the current mode control.

The effects of the local voltage feedback on audio-susceptibility are illustrated in Figs. 10(b) and 10(c). The numerator of audio-susceptibility, given by (17), has two resonances, the first determined by L_1' and C_2, and the second determined by L_2 and C_1'. For two-loop control, while the first resonance is eliminated by absorbing this resonance into the overall loop gain, the second resonance is still apparent in the audio-susceptibility, resulting in the peaking of Fig. 10(b). On the other hand, for three-loop control, both the first and second resonances are eliminated by absorbing these two resonances into the overall loop gain with a local voltage feedback, as shown in Fig. 10(c).

The audio-susceptibility and trans-impedance are compared in Figs. 11(a) and 11(b). For two-loop control, both trans-impedance and audio-susceptibility show some peaking. As mentioned previously, these peakings are a result of the resonance between L_2 and C_1' , and are inherent to the two-loop control. For three-loop control, the peakings are totally eliminated by absorbing the resonance between L_2 and C_1' into the control-loop with the local voltage feedback.

The output impedance characteristics of two converters are compared in Fig. 11(c). As expected, the output impedance is not significantly affected by the local voltage feedback. They have almost identical peak values and first corner frequencies, which determine the overshoot and the settling time of the step load response shown in Fig. 11(d) [8].

The outer loop gains are compared in Fig. 12. For the two-loop control, the resonance between L_2 and C_1' is apparent in this loop gain. This resonance strongly affects the phase and gain margin of the loop gain. To maintain adequate stability margins, the crossover frequency should be sufficiently lower than this resonance. For three-loop control, the resonance between L_2 and C_1' is no longer appar-

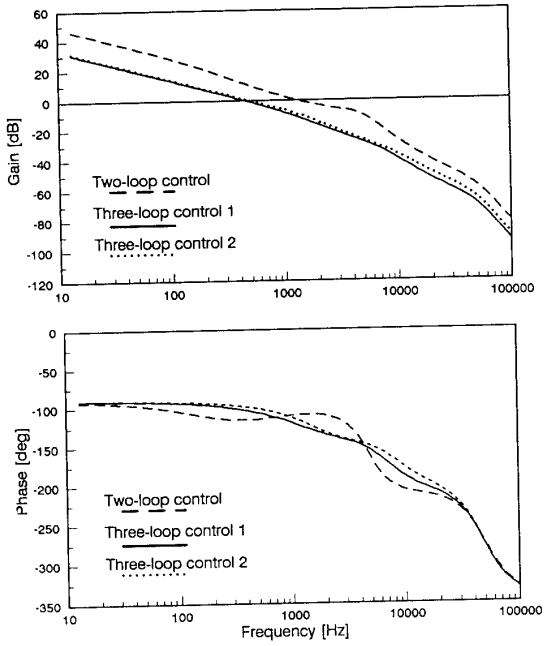

Fig. 12. Outer loop gain

ent in the loop gain (as expected from Fig. 9(b)), and consequently does not impose any direct constraint on the control-loop design. The magnitude of the loop gain is significantly reduced, resulting in a lower crossover frequency than for a two-loop control. However, the lower crossover frequency by no means indicates any degradation of the closed-loop performance.

Figures 13(a) and 13(b) show the trans-impedance and the module-failure response of output voltage (switch-open failure of the third converter module at 0.2 mSec). For the two-loop control, the larger peak of the trans-impedance results in a relatively large undershoot of transient response. For the three-loop control, the undershoot is significantly reduced with a smaller peak value of trans-impedance. In a module-failure response, since the disturbance of current at the summing junction of converter modules is a linear type (due to the opening of power switch) rather than an abrupt step change, the relationship between the trans-impedance and module-failure response is not so apparent as that between output impedance and step load response. However, there is still a certain dependency of the magnitude of undershoot and response time of the module-failure response on the peak value and the first corner of the trans-impedance. The lower peak value and the smaller first corner frequency of the trans-impedance indicate a smaller undershoot and a faster response. Figure 13(c) shows the inductor current waveform of the first converter module. For two-loop control, the inductor current responds with a certain delay, and it increases gradually to

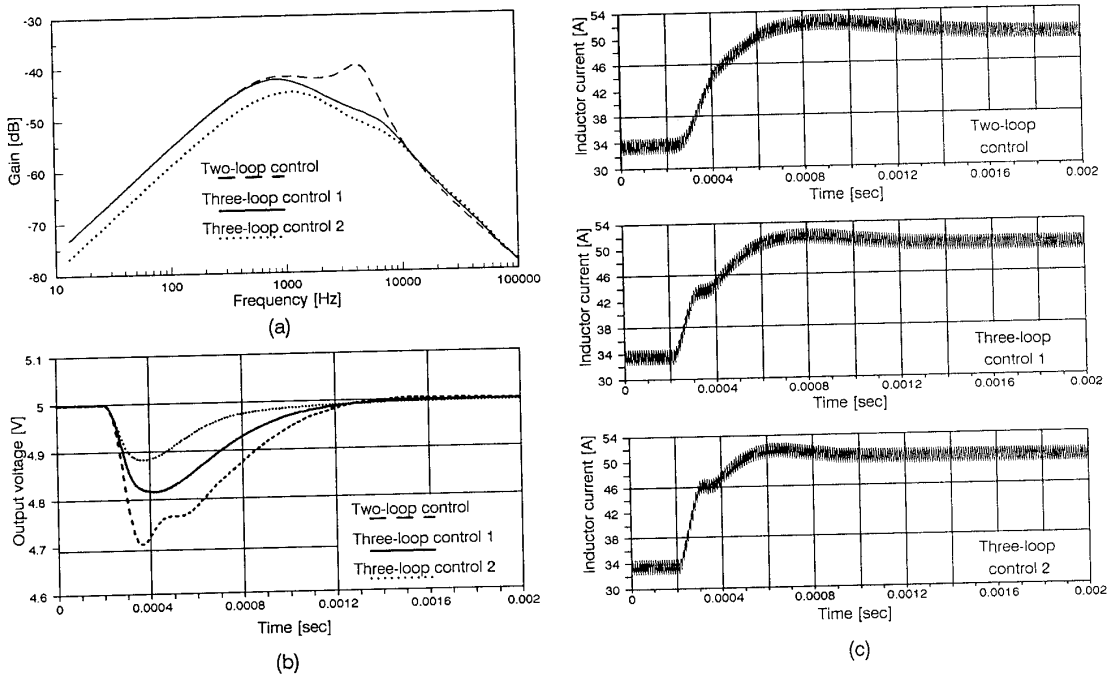

Fig. 13. Performances of a three-loop controlled converter: (a) Trans-impedance (b) Module-failure response of output (c) Module-failure response of inductor current

supplement the load current of the failed converter module. On the other hand, for three-loop control, the inductor current responds immediately.

5.2 Further improvement of performance

The transient responses and other closed-loop performance of three-loop-controlled converter can be further improved without compromising the stability. For example, the remote voltage and local voltage feedback gains are increased from the previous design, resulting in an improved design referred to as **three-loop control 2** in Figs. 10 through 13. While the small-signal performance and the transient response are significantly improved with the new design, the outer loop gains in Fig. 12 are unchanged up to the crossover frequency, having the same stability margins. Up to the crossover frequency, the outer loop gain is approximately proportional to the ratio of the remote and the local voltage feedback gain. Thus the simultaneous increase of two feedback gains does not significantly affect the outer loop gain until the crossover. This is quite different from the two-loop control, and again, it illustrates the benefits of local voltage feedback.

6. CONCLUSIONS

A systematic control-loop design procedure for a multi-module converter system is presented. First, a small-signal model of the system is derived using the PWM switch model and the small-signal model of the current mode control. Secondly, the small-signal model for the multi-module converter system is simplified to an equivalent single-module model. Finally, the control-loop design is implemented using the single-module model.

A three-loop control strategy for the multi-module converter system with a secondary output filter is developed. Significant improvements on small-signal performance and module-failure response are achieved using additional feedback from the intermediate filter stage.

The small-signal analysis of the three-loop controlled converter is performed, focusing on the effects of the local voltage feedback on the closed-loop performance of the system. It is shown that local voltage feedback minimizes any detrimental effect of the resonance between the power stage filter of each converter module and the common output filter.

The superiority of the three-loop control over the conventional two-loop control is discussed, and is substantiated by small-signal analysis and large-signal simulations. The effectiveness of the local-voltage feedback in improving the module-failure response is demonstrated by large signal simulations.

ACKNOWLEDGEMENTS

The authors express the gratitude to IBM-Kingston for many valuable discussions through the course of research and their suggestion of the three-loop control scheme for the multi-module converter system.

REFERENCES

[1] R.B. Ridley, "Small-Signal Analysis of Parallel Power Converters," M.S. Thesis, VPI&SU, March 1986

[2] R.B. Ridley, "Secondary LC Filter Analysis and Design Techniques for Current-Mode-Controlled Converters," IEEE Transactions on Power Electronics, October 1988

[3] V. Vorperian, R. Tymerski and F.C. Lee, "Equivalent Circuit Models for Resonant and PWM Switches," IEEE Transactions on Power Electronics, April 1989

[4] V. Vorperian, "Simplified Analysis of PWM Converters Using the Model of the PWM Switch," IEEE Transactions on AES, March 1990

[5] R.B. Ridley, "A New Continuous-Time Model for Current Mode Control," Power Conversion and Intelligent Motion Conference, November 1989

[6] B.H. Cho and F.C. Lee, "Measurement of Loop Gain with the Digital Modulator," IEEE Transaction on Power Electronics, January 1986

[7] R.B. Ridley, B.H. Cho and F.C. Lee, "Analysis and Interpretation of Loop Gains of Multi-Loop-Controlled Switching Regulator," IEEE Transactions on Power Electronics, October 1988

[8] F.C. Lee, Y. Yu, and M.F. Mahmoud, "A Unified Analysis and Design Procedure for a Standardized Control Module for DC-DC Switching Regulator," Power Electronics Specialists Conference, June 1980